

Search for a Higgs Boson in the Diphoton Final State in $p\bar{p}$ Collisions at $\sqrt{s} = 1.96$ TeV

T. Aaltonen,²¹ B. Álvarez González^{w,9}, S. Amerio,⁴¹ D. Amidei,³² A. Anastassov,³⁶ A. Annovi,¹⁷ J. Antos,¹² G. Apollinari,¹⁵ J.A. Appel,¹⁵ A. Apresyan,⁴⁶ T. Arisawa,⁵⁶ A. Artikov,¹³ J. Asaadi,⁵¹ W. Ashmanskas,¹⁵ B. Auerbach,⁵⁹ A. Aurisano,⁵¹ F. Azfar,⁴⁰ W. Badgett,¹⁵ A. Barbaro-Galtieri,²⁶ V.E. Barnes,⁴⁶ B.A. Barnett,²³ P. Barria^{dd,44} P. Bartos,¹² M. Bauce^{bb,41} G. Bauer,³⁰ F. Bedeschi,⁴⁴ D. Beecher,²⁸ S. Behari,²³ G. Bellettini^{cc,44} J. Bellinger,⁵⁸ D. Benjamin,¹⁴ A. Beretvas,¹⁵ A. Bhatti,⁴⁸ M. Binkley,^{15,*} D. Bisello^{bb,41} I. Bizjak^{hh,28} K.R. Bland,⁵ B. Blumenfeld,²³ A. Bocci,¹⁴ A. Bodek,⁴⁷ D. Bortoletto,⁴⁶ J. Boudreau,⁴⁵ A. Boveia,¹¹ L. Brigliadori^{aa,6} A. Brisuda,¹² C. Bromberg,³³ E. Brucken,²¹ M. Bucchiantonio^{cc,44} J. Budagov,¹³ H.S. Budd,⁴⁷ S. Budd,²² K. Burkett,¹⁵ G. Busetto^{bb,41} P. Bussey,¹⁹ A. Buzatu,³¹ C. Calancha,²⁹ S. Camarda,⁴ M. Campanelli,²⁸ M. Campbell,³² F. Canelli^{11,15} B. Carls,²² D. Carlsmith,⁵⁸ R. Carosi,⁴⁴ S. Carrillo^{k,16} S. Carron,¹⁵ B. Casal,⁹ M. Casarsa,¹⁵ A. Castro^{aa,6} P. Catastini,²⁰ D. Cauz,⁵² V. Cavaliere,²² M. Cavalli-Sforza,⁴ A. Cerri^{e,26} L. Cerrito^{q,28} Y.C. Chen,¹ M. Chertok,⁷ G. Chiarelli,⁴⁴ G. Chlachidze,¹⁵ F. Chlebana,¹⁵ K. Cho,²⁵ D. Chokheli,¹³ J.P. Chou,²⁰ W.H. Chung,⁵⁸ Y.S. Chung,⁴⁷ C.I. Ciobanu,⁴² M.A. Ciocci^{dd,44} A. Clark,¹⁸ C. Clarke,⁵⁷ G. Compostella^{bb,41} M.E. Convery,¹⁵ J. Conway,⁷ M. Corbo,⁴² M. Cordelli,¹⁷ C.A. Cox,⁷ D.J. Cox,⁷ F. Crescioli^{cc,44} C. Cuenca Almenar,⁵⁹ J. Cuevas^{w,9} R. Culbertson,¹⁵ D. Dagenhart,¹⁵ N. d'Ascenzo^{u,42} M. Datta,¹⁵ P. de Barbaro,⁴⁷ S. De Cecco,⁴⁹ G. De Lorenzo,⁴ M. Dell'Orso^{cc,44} C. Deluca,⁴ L. Demortier,⁴⁸ J. Deng^{b,14} M. Deninno,⁶ F. Devoto,²¹ M. d'Errico^{bb,41} A. Di Canto^{cc,44} B. Di Ruzza,⁴⁴ J.R. Dittmann,⁵ M. D'Onofrio,²⁷ S. Donati^{cc,44} P. Dong,¹⁵ M. Dorigo,⁵² T. Dorigo,⁴¹ K. Ebina,⁵⁶ A. Elagin,⁵¹ A. Eppig,³² R. Erbacher,⁷ D. Errede,²² S. Errede,²² N. Ershaidat^{z,42} R. Eusebi,⁵¹ H.C. Fang,²⁶ S. Farrington,⁴⁰ M. Feindt,²⁴ J.P. Fernandez,²⁹ C. Ferrazza^{ee,44} R. Field,¹⁶ G. Flanagan^{s,46} R. Forrest,⁷ M.J. Frank,⁵ M. Franklin,²⁰ J.C. Freeman,¹⁵ Y. Funakoshi,⁵⁶ I. Furic,¹⁶ M. Gallinaro,⁴⁸ J. Galyardt,¹⁰ J.E. Garcia,¹⁸ A.F. Garfinkel,⁴⁶ P. Garosi^{dd,44} H. Gerberich,²² E. Gerchtein,¹⁵ S. Giagu^{ff,49} V. Giakoumopoulou,³ P. Giannetti,⁴⁴ K. Gibson,⁴⁵ C.M. Ginsburg,¹⁵ N. Giokaris,³ P. Giromini,¹⁷ M. Giunta,⁴⁴ G. Giurgiu,²³ V. Glagolev,¹³ D. Glenzinski,¹⁵ M. Gold,³⁵ D. Goldin,⁵¹ N. Goldschmidt,¹⁶ A. Golossanov,¹⁵ G. Gomez,⁹ G. Gomez-Ceballos,³⁰ M. Goncharov,³⁰ O. González,²⁹ I. Gorelov,³⁵ A.T. Goshaw,¹⁴ K. Goulianos,⁴⁸ S. Grinstein,⁴ C. Grosso-Pilcher,¹¹ R.C. Group^{55,15} J. Guimaraes da Costa,²⁰ Z. Gunay-Unalan,³³ C. Haber,²⁶ S.R. Hahn,¹⁵ E. Halkiadakis,⁵⁰ A. Hamaguchi,³⁹ J.Y. Han,⁴⁷ F. Happacher,¹⁷ K. Hara,⁵³ D. Hare,⁵⁰ M. Hare,⁵⁴ R.F. Harr,⁵⁷ K. Hatakeyama,⁵ C. Hays,⁴⁰ M. Heck,²⁴ J. Heinrich,⁴³ M. Herndon,⁵⁸ S. Hewamanage,⁵ D. Hidas,⁵⁰ A. Hocker,¹⁵ W. Hopkins^{f,15} D. Horn,²⁴ S. Hou,¹ R.E. Hughes,³⁷ M. Hurwitz,¹¹ U. Husemann,⁵⁹ N. Hussain,³¹ M. Hussein,³³ J. Huston,³³ G. Introzzi,⁴⁴ M. Iori^{ff,49} A. Ivanov^{o,7} E. James,¹⁵ D. Jang,¹⁰ B. Jayatilaka,¹⁴ E.J. Jeon,²⁵ M.K. Jha,⁶ S. Jindariani,¹⁵ W. Johnson,⁷ M. Jones,⁴⁶ K.K. Joo,²⁵ S.Y. Jun,¹⁰ T.R. Junk,¹⁵ T. Kamon,⁵¹ P.E. Karchin,⁵⁷ A. Kasmi,⁵ Y. Kato^{n,39} W. Ketchum,¹¹ J. Keung,⁴³ V. Khotilovich,⁵¹ B. Kilminster,¹⁵ D.H. Kim,²⁵ H.S. Kim,²⁵ H.W. Kim,²⁵ J.E. Kim,²⁵ M.J. Kim,¹⁷ S.B. Kim,²⁵ S.H. Kim,⁵³ Y.K. Kim,¹¹ N. Kimura,⁵⁶ M. Kirby,¹⁵ S. Klimenko,¹⁶ K. Kondo,^{56,*} D.J. Kong,²⁵ J. Konigsberg,¹⁶ A.V. Kotwal,¹⁴ M. Kreps,²⁴ J. Kroll,⁴³ D. Krop,¹¹ N. Krumnack^{l,5} M. Kruse,¹⁴ V. Krutelyov^{c,51} T. Kuhr,²⁴ M. Kurata,⁵³ S. Kwang,¹¹ A.T. Laasanen,⁴⁶ S. Lami,⁴⁴ S. Lammel,¹⁵ M. Lancaster,²⁸ R.L. Lander,⁷ K. Lannon^{v,37} A. Lath,⁵⁰ G. Latino^{cc,44} T. LeCompte,² E. Lee,⁵¹ H.S. Lee,¹¹ J.S. Lee,²⁵ S.W. Lee^{x,51} S. Leo^{cc,44} S. Leone,⁴⁴ J.D. Lewis,¹⁵ A. Limosani^{r,14} C.-J. Lin,²⁶ J. Linacre,⁴⁰ M. Lindgren,¹⁵ E. Lipeles,⁴³ A. Lister,¹⁸ D.O. Litvintsev,¹⁵ C. Liu,⁴⁵ Q. Liu,⁴⁶ T. Liu,¹⁵ S. Lockwitz,⁵⁹ A. Loginov,⁵⁹ D. Lucchesi^{bb,41} J. Lueck,²⁴ P. Lujan,²⁶ P. Lukens,¹⁵ G. Lungu,⁴⁸ J. Lys,²⁶ R. Lysak,¹² R. Madrak,¹⁵ K. Maeshima,¹⁵ K. Makhoul,³⁰ S. Malik,⁴⁸ G. Manca^{a,27} A. Manousakis-Katsikakis,³ F. Margaroli,⁴⁶ C. Marino,²⁴ M. Martínez,⁴ R. Martínez-Ballarín,²⁹ P. Mastrandrea,⁴⁹ M.E. Mattson,⁵⁷ P. Mazzanti,⁶ K.S. McFarland,⁴⁷ P. McIntyre,⁵¹ R. McNulty^{i,27} A. Mehta,²⁷ P. Mehtala,²¹ A. Menzione,⁴⁴ C. Mesropian,⁴⁸ T. Miao,¹⁵ D. Mietlicki,³² A. Mitra,¹ H. Miyake,⁵³ S. Moed,²⁰ N. Moggi,⁶ M.N. Mondragon^{k,15} C.S. Moon,²⁵ R. Moore,¹⁵ M.J. Morello,¹⁵ J. Morlock,²⁴ P. Movilla Fernandez,¹⁵ A. Mukherjee,¹⁵ Th. Muller,²⁴ P. Murat,¹⁵ M. Mussini^{aa,6} J. Nachtman^{m,15} Y. Nagai,⁵³ J. Naganoma,⁵⁶ I. Nakano,³⁸ A. Napier,⁵⁴ J. Nett,⁵¹ C. Neu,⁵⁵ M.S. Neubauer,²² J. Nielsen^{d,26} L. Nodulman,² O. Norriella,²² E. Nurse,²⁸ L. Oakes,⁴⁰ S.H. Oh,¹⁴ Y.D. Oh,²⁵ I. Oksuzian,⁵⁵ T. Okusawa,³⁹ R. Orava,²¹ L. Ortolan,⁴ S. Pagan Griso^{bb,41} C. Pagliarone,⁵² E. Palencia^{e,9} V. Papadimitriou,¹⁵ A.A. Paramonov,² J. Patrick,¹⁵ G. Pauletta^{gg,52} M. Paulini,¹⁰ C. Paus,³⁰ D.E. Pellett,⁷ A. Penzo,⁵² T.J. Phillips,¹⁴ G. Piacentino,⁴⁴ E. Pianori,⁴³ J. Pilot,³⁷ K. Pitts,²² C. Plager,⁸ L. Pondrom,⁵⁸ S. Poprocki^{f,15} K. Potamianos,⁴⁶ O. Poukhov,^{13,*}

F. Prokoshin^{y,13} A. Pronko,¹⁵ F. Ptohos^{g,17} E. Pueschel,¹⁰ G. Punzi^{cc,44} J. Pursley,⁵⁸ A. Rahaman,⁴⁵ V. Ramakrishnan,⁵⁸ N. Ranjan,⁴⁶ J. Ray,¹⁵ I. Redondo,²⁹ P. Renton,⁴⁰ M. Rescigno,⁴⁹ T. Riddick,²⁸ F. Rimondi^{aa,6} L. Ristori^{44,15} A. Robson,¹⁹ T. Rodrigo,⁹ T. Rodriguez,⁴³ E. Rogers,²² S. Rolli^{h,54} R. Roser,¹⁵ M. Rossi,⁵² F. Rubbo,¹⁵ F. Ruffini^{dd,44} A. Ruiz,⁹ J. Russ,¹⁰ V. Rusu,¹⁵ A. Safonov,⁵¹ W.K. Sakumoto,⁴⁷ Y. Sakurai,⁵⁶ L. Santi^{gg,52} L. Sartori,⁴⁴ K. Sato,⁵³ V. Saveliev^{u,42} A. Savoy-Navarro,⁴² P. Schlabach,¹⁵ A. Schmidt,²⁴ E.E. Schmidt,¹⁵ M.P. Schmidt,^{59,*} M. Schmitt,³⁶ T. Schwarz,⁷ L. Scodellaro,⁹ A. Scribano^{dd,44} F. Scuri,⁴⁴ A. Sedov,⁴⁶ S. Seidel,³⁵ Y. Seiya,³⁹ A. Semenov,¹³ F. Sforza^{cc,44} A. Sfyrla,²² S.Z. Shalhout,⁷ T. Shears,²⁷ P.F. Shepard,⁴⁵ M. Shimojima^{t,53} S. Shiraishi,¹¹ M. Shochet,¹¹ I. Shreyber,³⁴ A. Simonenko,¹³ P. Sinervo,³¹ A. Sissakian,^{13,*} K. Sliwa,⁵⁴ J.R. Smith,⁷ F.D. Snider,¹⁵ A. Soha,¹⁵ S. Somalwar,⁵⁰ V. Sorin,⁴ P. Squillacioti,⁴⁴ M. Stancari,¹⁵ M. Stanitzki,⁵⁹ R. St. Denis,¹⁹ B. Stelzer,³¹ O. Stelzer-Chilton,³¹ D. Stentz,³⁶ J. Strologas,³⁵ G.L. Strycker,³² Y. Sudo,⁵³ A. Sukhanov,¹⁶ I. Suslov,¹³ K. Takemasa,⁵³ Y. Takeuchi,⁵³ J. Tang,¹¹ M. Tecchio,³² P.K. Teng,¹ J. Thom^{f,15} J. Thome,¹⁰ G.A. Thompson,²² E. Thomson,⁴³ P. Ttito-Guzmán,²⁹ S. Tkaczyk,¹⁵ D. Toback,⁵¹ S. Tokar,¹² K. Tollefson,³³ T. Tomura,⁵³ D. Tonelli,¹⁵ S. Torre,¹⁷ D. Torretta,¹⁵ P. Totaro,⁴¹ M. Trovato^{ee,44} Y. Tu,⁴³ F. Ukegawa,⁵³ S. Uozumi,²⁵ A. Varganov,³² F. Vázquez^{k,16} G. Velev,¹⁵ C. Vellidis,³ M. Vidal,²⁹ I. Vila,⁹ R. Vilar,⁹ J. Vizán,⁹ M. Vogel,³⁵ G. Volpi^{cc,44} P. Wagner,⁴³ R.L. Wagner,¹⁵ T. Wakisaka,³⁹ R. Wallny,⁸ S.M. Wang,¹ A. Warburton,³¹ D. Waters,²⁸ M. Weinberger,⁵¹ W.C. Wester III,¹⁵ B. Whitehouse,⁵⁴ D. Whiteson^{b,43} A.B. Wicklund,² E. Wicklund,¹⁵ S. Wilbur,¹¹ F. Wick,²⁴ H.H. Williams,⁴³ J.S. Wilson,³⁷ P. Wilson,¹⁵ B.L. Winer,³⁷ P. Wittich^{f,15} S. Wolbers,¹⁵ H. Wolfe,³⁷ T. Wright,³² X. Wu,¹⁸ Z. Wu,⁵ K. Yamamoto,³⁹ J. Yamaoka,¹⁴ T. Yang,¹⁵ U.K. Yang^{p,11} Y.C. Yang,²⁵ W.-M. Yao,²⁶ G.P. Yeh,¹⁵ K. Yi^{m,15} J. Yoh,¹⁵ K. Yorita,⁵⁶ T. Yoshida^{j,39} G.B. Yu,¹⁴ I. Yu,²⁵ S.S. Yu,¹⁵ J.C. Yun,¹⁵ A. Zanetti,⁵² Y. Zeng,¹⁴ and S. Zucchelli^{aa,6}

(CDF Collaboration)[†]

¹*Institute of Physics, Academia Sinica, Taipei, Taiwan 11529, Republic of China*

²*Argonne National Laboratory, Argonne, Illinois 60439, USA*

³*University of Athens, 157 71 Athens, Greece*

⁴*Institut de Física d'Altes Energies, ICREA, Universitat Autònoma de Barcelona, E-08193, Bellaterra (Barcelona), Spain*

⁵*Baylor University, Waco, Texas 76798, USA*

⁶*Istituto Nazionale di Fisica Nucleare Bologna, ^{aa}University of Bologna, I-40127 Bologna, Italy*

⁷*University of California, Davis, Davis, California 95616, USA*

⁸*University of California, Los Angeles, Los Angeles, California 90024, USA*

⁹*Instituto de Física de Cantabria, CSIC-University of Cantabria, 39005 Santander, Spain*

¹⁰*Carnegie Mellon University, Pittsburgh, Pennsylvania 15213, USA*

¹¹*Enrico Fermi Institute, University of Chicago, Chicago, Illinois 60637, USA*

¹²*Comenius University, 842 48 Bratislava, Slovakia; Institute of Experimental Physics, 040 01 Kosice, Slovakia*

¹³*Joint Institute for Nuclear Research, RU-141980 Dubna, Russia*

¹⁴*Duke University, Durham, North Carolina 27708, USA*

¹⁵*Fermi National Accelerator Laboratory, Batavia, Illinois 60510, USA*

¹⁶*University of Florida, Gainesville, Florida 32611, USA*

¹⁷*Laboratori Nazionali di Frascati, Istituto Nazionale di Fisica Nucleare, I-00044 Frascati, Italy*

¹⁸*University of Geneva, CH-1211 Geneva 4, Switzerland*

¹⁹*Glasgow University, Glasgow G12 8QQ, United Kingdom*

²⁰*Harvard University, Cambridge, Massachusetts 02138, USA*

²¹*Division of High Energy Physics, Department of Physics, University of Helsinki and Helsinki Institute of Physics, FIN-00014, Helsinki, Finland*

²²*University of Illinois, Urbana, Illinois 61801, USA*

²³*The Johns Hopkins University, Baltimore, Maryland 21218, USA*

²⁴*Institut für Experimentelle Kernphysik, Karlsruhe Institute of Technology, D-76131 Karlsruhe, Germany*

²⁵*Center for High Energy Physics: Kyungpook National University,*

Daegu 702-701, Korea; Seoul National University, Seoul 151-742,

Korea; Sungkyunkwan University, Suwon 440-746,

Korea; Korea Institute of Science and Technology Information,

Daejeon 305-806, Korea; Chonnam National University, Gwangju 500-757,

Korea; Chonbuk National University, Jeonju 561-756, Korea

²⁶*Ernest Orlando Lawrence Berkeley National Laboratory, Berkeley, California 94720, USA*

²⁷*University of Liverpool, Liverpool L69 7ZE, United Kingdom*

²⁸*University College London, London WC1E 6BT, United Kingdom*

²⁹*Centro de Investigaciones Energeticas Medioambientales y Tecnológicas, E-28040 Madrid, Spain*

³⁰*Massachusetts Institute of Technology, Cambridge, Massachusetts 02139, USA*

- ³¹*Institute of Particle Physics: McGill University, Montréal, Québec, Canada H3A 2T8; Simon Fraser University, Burnaby, British Columbia, Canada V5A 1S6; University of Toronto, Toronto, Ontario, Canada M5S 1A7; and TRIUMF, Vancouver, British Columbia, Canada V6T 2A3*
- ³²*University of Michigan, Ann Arbor, Michigan 48109, USA*
- ³³*Michigan State University, East Lansing, Michigan 48824, USA*
- ³⁴*Institution for Theoretical and Experimental Physics, ITEP, Moscow 117259, Russia*
- ³⁵*University of New Mexico, Albuquerque, New Mexico 87131, USA*
- ³⁶*Northwestern University, Evanston, Illinois 60208, USA*
- ³⁷*The Ohio State University, Columbus, Ohio 43210, USA*
- ³⁸*Okayama University, Okayama 700-8530, Japan*
- ³⁹*Osaka City University, Osaka 588, Japan*
- ⁴⁰*University of Oxford, Oxford OX1 3RH, United Kingdom*
- ⁴¹*Istituto Nazionale di Fisica Nucleare, Sezione di Padova-Trento,* ^{bb}*University of Padova, I-35131 Padova, Italy*
- ⁴²*LPNHE, Universite Pierre et Marie Curie/IN2P3-CNRS, UMR7585, Paris, F-75252 France*
- ⁴³*University of Pennsylvania, Philadelphia, Pennsylvania 19104, USA*
- ⁴⁴*Istituto Nazionale di Fisica Nucleare Pisa,* ^{cc}*University of Pisa,*
- ^{dd}*University of Siena and* ^{ee}*Scuola Normale Superiore, I-56127 Pisa, Italy*
- ⁴⁵*University of Pittsburgh, Pittsburgh, Pennsylvania 15260, USA*
- ⁴⁶*Purdue University, West Lafayette, Indiana 47907, USA*
- ⁴⁷*University of Rochester, Rochester, New York 14627, USA*
- ⁴⁸*The Rockefeller University, New York, New York 10065, USA*
- ⁴⁹*Istituto Nazionale di Fisica Nucleare, Sezione di Roma 1,*
- ^{ff}*Sapienza Università di Roma, I-00185 Roma, Italy*
- ⁵⁰*Rutgers University, Piscataway, New Jersey 08855, USA*
- ⁵¹*Texas A&M University, College Station, Texas 77843, USA*
- ⁵²*Istituto Nazionale di Fisica Nucleare Trieste/Udine,*
- ^{gg}*I-34100 Trieste,* ⁹⁹*University of Udine, I-33100 Udine, Italy*
- ⁵³*University of Tsukuba, Tsukuba, Ibaraki 305, Japan*
- ⁵⁴*Tufts University, Medford, Massachusetts 02155, USA*
- ⁵⁵*University of Virginia, Charlottesville, Virginia 22906, USA*
- ⁵⁶*Waseda University, Tokyo 169, Japan*
- ⁵⁷*Wayne State University, Detroit, Michigan 48201, USA*
- ⁵⁸*University of Wisconsin, Madison, Wisconsin 53706, USA*
- ⁵⁹*Yale University, New Haven, Connecticut 06520, USA*
- (Dated: September 21, 2011)

A search for a narrow Higgs boson resonance in the diphoton mass spectrum is presented based on data corresponding to 7.0 fb^{-1} of integrated luminosity from $p\bar{p}$ collisions at $\sqrt{s} = 1.96 \text{ TeV}$ collected by the CDF experiment. No evidence of such a resonance is observed, and upper limits are set on the cross section times branching ratio of the resonant state as a function of Higgs boson mass. The limits are interpreted in the context of the standard model and one fermiophobic benchmark model where the data exclude fermiophobic Higgs bosons with masses below $114 \text{ GeV}/c^2$ at a 95% Bayesian credibility level.

PACS numbers: 12.38.Qk, 13.85.Rm, 14.80.Bn, 14.80.Ec, 12.60.Fr

In the standard model (SM) of particle physics, the electromagnetic and weak forces are unified into a single theory known as electroweak theory. However, the measured cross sections for electromagnetic and weak interactions differ by several orders of magnitude due to massive W and Z bosons that mediate the weak interactions. These bosons gain mass via electroweak symmetry breaking by way of the Higgs mechanism [1], and the electroweak theory predicts the existence of a boson, known as the Higgs boson, that provides a direct test of the theory.

The SM prediction for the Higgs boson branching ratio into a photon pair $\mathcal{B}(H \rightarrow \gamma\gamma)$ is extremely small, reaching a maximal value of only about 0.2% for a Higgs

boson mass $m_H = 120 \text{ GeV}/c^2$ [2]. Even so, a search using the diphoton final state is appealing due to its better mass resolution and reconstruction efficiency relative to dominant decay modes involving b quarks. The $H \rightarrow \gamma\gamma$ channel provides its greatest sensitivity for Higgs boson masses between 110 and 140 GeV/c^2 , contributing in a region most useful to combined Tevatron Higgs boson searches [3] and overlapping with a region preferred by electroweak constraints [4]. In addition, in “fermiophobic” Higgs boson models, where the coupling of the Higgs boson to fermions is suppressed, the diphoton decay can be greatly enhanced [5].

The Collider Detector at Fermilab (CDF) and D0 experiments at the Tevatron have searched for both a SM

Higgs boson and a fermiophobic Higgs boson h_f decaying to two photons [6–8]. The D0 experiment recently set 95% confidence level (C.L.) upper limits on the cross section times branching ratio $\sigma \times \mathcal{B}(H \rightarrow \gamma\gamma)$ relative to the SM prediction and on $\mathcal{B}(h_f \rightarrow \gamma\gamma)$ using data corresponding to an integrated luminosity \mathcal{L} of 8.2 fb^{-1} [9]. The h_f result sets a lower limit on m_{h_f} of $112.9 \text{ GeV}/c^2$, a more stringent limit than that of $109.7 \text{ GeV}/c^2$ obtained from combined searches at the LEP electron-positron collider at CERN [5]. Previously, the CDF experiment set 95% C.L. upper limits on $\mathcal{B}(h_f \rightarrow \gamma\gamma)$ with data corresponding to $\mathcal{L} = 3.0 \text{ fb}^{-1}$, resulting in an exclusion of m_{h_f} below $106 \text{ GeV}/c^2$ [10].

In this Letter, we present a search of the diphoton mass distribution from CDF data for a narrow resonance that could reveal the presence of a SM or fermiophobic Higgs boson. This analysis, which uses more than twice the integrated luminosity of the previous CDF h_f analysis [10], implements new techniques to improve the identification of photons and yields a new, improved lower limit on the fermiophobic Higgs boson mass. In addition, this is the first search for the SM Higgs boson at CDF using $H \rightarrow \gamma\gamma$ decays from Run II data.

The SM Higgs production mechanisms considered in this study are gluon fusion (GF), associated production (VH) where a Higgs boson is produced in association with a W or Z boson, and vector boson fusion (VBF) with cross sections of 1072.3 fb [11], 240.3 fb [12], and 72.7 fb [13], respectively, for $m_H = 120 \text{ GeV}/c^2$. A benchmark fermiophobic model is considered in which the Higgs boson does not couple to fermions, yet retains its SM couplings to bosons [5]. In this model, the GF process is suppressed and the fermiophobic Higgs boson production is dominated by VH and VBF. Furthermore, Higgs boson decays to fermions are removed, resulting in increased branching ratios for decays into gauge bosons.

We use the CDF II detector [14] to identify photon candidate events produced in $p\bar{p}$ collisions at $\sqrt{s} = 1.96 \text{ TeV}$. The silicon vertex tracker [15] and the central outer tracker [16], contained within a 1.4 T axial magnetic field, measure the trajectories of charged particles and determine their momenta. Particles that pass through the central outer tracker reach the electromagnetic (EM) and hadronic calorimeters [17–19], which are divided into two regions: central ($|\eta| < 1.1$) [20] and forward or “plug” ($1.1 < |\eta| < 3.6$). The EM calorimeters contain fine-grained shower maximum detectors [21], which measure the shower shape and centroid position in the two dimensions transverse to the direction of the shower development.

Events with two photon candidates are selected, and the data are divided into four categories according to the position and type of the photons. In central-central (CC) events, both photon candidates are located within the fiducial region of the central EM calorimeter ($|\eta| < 1.05$); in central-plug (CP) events, one photon candidate is lo-

cated in this region and the other is in the fiducial region of the plug calorimeter ($1.2 < |\eta| < 2.8$); in central-central events with a conversion (C’C), both photon candidates are in the central region, but one photon converts and is reconstructed from its e^+e^- decay products; and, in central-plug events with a conversion (C’P), there is one central conversion candidate together with a plug photon candidate.

The events are selected by a three-level trigger system that requires an isolated cluster of energy deposited in the EM calorimeter with a transverse energy $E_T > 25 \text{ GeV}$ [22]. The trigger efficiency for events accepted into the final sample is determined from simulation and found to be essentially 100% for the most sensitive event category (CC) and above 90% for all other categories.

A set of selection criteria is used to remove background events and to identify high-energy photon candidates for this analysis. All reconstructed photon candidates are required to have $E_T > 15 \text{ GeV}$. Plug photon candidates are identified using standard CDF requirements described elsewhere [23, 24]. A new neural network (NN) technique is used to identify photons in the central region. Central photon candidates are first required to satisfy loose selection requirements, as described in Ref. [25]. After additional track requirements are applied to remove electrons, the remaining candidates are required to have a NN output value above a threshold that is selected to maximize $H \rightarrow \gamma\gamma$ sensitivity. As more than half of the events in the data with two photon candidates contain either one or two jets misidentified as a prompt photon [26], the NN discriminant is trained using photon and jet Monte Carlo (MC) samples and constructed from several detector variables that distinguish true photons from these jet backgrounds [27]. These variables include the ratio of energy in the shower maximum detector to that in the calorimeter cluster associated with the photon, the ratio of hadronic to EM transverse energy, calorimeter and track isolation [25], and a χ^2 value calculated by comparing the measured transverse shower profile to that of a single EM shower [28]. This NN method increases the photon signal efficiency by $\sim 5\%$ and background rejection by $\sim 12\%$ compared to the standard selection requirements for central photons [25], which improves $H \rightarrow \gamma\gamma$ sensitivity by about 9%.

As photons pass through the CDF detector material, EM interactions with a nucleus cause about 15% of central photons to convert into an electron-positron pair. In order to recover these conversion photons, we search for a central electron with a nearby track corresponding to a particle of opposite charge. The proximity of the two tracks is first determined by requiring the transverse distance between the two tracks to be less than 0.2 cm at the radial location where they are parallel. The difference in $\cot\theta$ between the two tracks must be less than 0.04, where $\cot\theta = p_z/p_T$. Backgrounds are further removed by requiring the ratio of E_T to p_T of the recon-

structured conversion photon to be between $0.1c$ and $1.9c$ and calorimeter isolation to be less than 2.6 GeV, where cut boundaries are optimized to maximize $H \rightarrow \gamma\gamma$ sensitivity. The direction of the conversion photon's momentum is obtained by taking the vector sum of the individual track momenta. Better $H \rightarrow \gamma\gamma$ mass resolution is obtained, however, by setting the total momentum to be the conversion photon's energy obtained from EM calorimeters. Reconstruction of photon conversions in this analysis provides an improvement of about 13% in sensitivity to a Higgs boson signal [29].

The above selection criteria define an inclusive diphoton sample for the SM Higgs boson search. In order to improve sensitivity for the fermiophobic Higgs boson search, the event selection is extended by taking advantage of the final-state features present in the VH and VBF processes. Because the Higgs boson from these processes will be produced with a W or Z boson or with two jets, the transverse momentum of the diphoton system $p_T^{\gamma\gamma}$ is generally higher relative to the diphoton backgrounds. A requirement of $p_T^{\gamma\gamma} > 75$ GeV/ c forms a region of high h_f sensitivity, retaining roughly 30% of the signal while removing 99.5% of the background [10]. Two lower $p_T^{\gamma\gamma}$ regions are additionally included and provide about 15% more h_f sensitivity: $p_T^{\gamma\gamma} < 35$ GeV/ c and 35 GeV/ $c < p_T^{\gamma\gamma} < 75$ GeV/ c . With four diphoton categories (CC, CP, C'C, and C'P) and three $p_T^{\gamma\gamma}$ regions, twelve independent channels are included for the fermiophobic Higgs boson search.

The efficiency times detector acceptance for signal events given in Table I [30] is calculated using PYTHIA [31] MC event samples, which are generated as described in Ref. [10]. Corrections in the photon identification (ID) efficiencies due to imperfections in the detector simulation are derived using electrons from Z boson decays by comparing the ID efficiencies obtained from the detector simulation to the ID efficiencies measured in the data [10]. For central conversions, a study of $Z \rightarrow e^\pm +$ trident events in data and MC is used to obtain a systematic uncertainty of 7% on the efficiency of conversion identification, where a trident is defined as an electron that radiates a photon via bremsstrahlung which then converts to an electron-positron pair ($e^\mp\gamma \rightarrow e^\mp e^+e^-$).

The largest systematic uncertainties on the expected number of Higgs boson events arise from the conversion ID efficiency (7%), the integrated luminosity measurement (6%), varying the parton distribution functions used in PYTHIA (up to 5%) [32, 33], varying the parameters that control the amount of initial- and final-state radiation from the parton shower model of PYTHIA (about 4%) [34], and the PYTHIA modeling of the shape of the $p_T^{\gamma\gamma}$ distribution for the h_f signal (up to 4%). The latter uncertainty is only for VH and VBF used in the fermiophobic search and was obtained by studying the effect on the acceptance from the differences in the shape of the $p_T^{\gamma\gamma}$ distribution from PYTHIA and from leading-order

TABLE I. Efficiency times detector acceptance (ϵA) for signal events in each event category (CC, CP, C'C, and C'P) for $m_H = 120$ GeV/ c^2 , as a percentage of the total number of $H \rightarrow \gamma\gamma$ decays for each production mechanism. For the h_f search, results for VH and VBF are shown for the high|medium|low $p_T^{\gamma\gamma}$ regions as described in the text.

ϵA (%)	H_{SM} Search			h_f Search		
	GF	VH	VBF	VH	VBF	VBF
CC	10.0	10.2	11.0	4.8 3.8 1.9	4.2 4.6 2.6	4.2 4.6 2.6
CP	12.0	10.9	11.1	4.2 4.7 2.5	3.6 5.0 3.0	3.6 5.0 3.0
C'C	2.4	2.3	2.6	1.0 0.9 0.4	0.9 1.0 0.6	0.9 1.0 0.6
C'P	1.4	1.2	1.2	0.4 0.5 0.3	0.3 0.5 0.3	0.3 0.5 0.3
Total	25.8	24.6	25.9	10.4 9.9 5.1	9.0 11.1 6.5	9.0 11.1 6.5

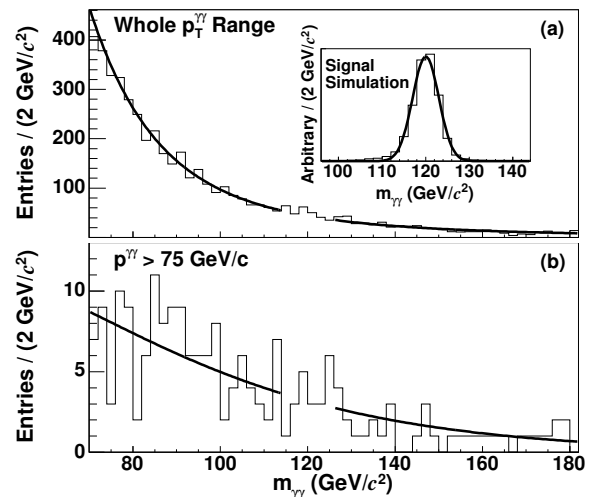


FIG. 1. The invariant mass distribution of the data for CC photon pairs is shown in (a) for the entire $p_T^{\gamma\gamma}$ region used in the SM Higgs boson search and (b) for the highest $p_T^{\gamma\gamma}$ region (the most sensitive region) used in the h_f search. Each distribution shows a fit to the data for the hypothesis of a m_H of 120 GeV/ c^2 . The gap in the fit centered at 120 GeV/ c^2 represents the signal region for this mass point that was excluded from the fit. The expected shape of the signal from simulation is shown in the inset of (a).

and next-to-leading-order calculations [35]. Finally, we include uncertainties from the photon ID efficiency (up to 4%), the trigger efficiency (less than 3%), and the EM energy scale (less than 1%).

The decay of a Higgs boson into a photon pair would appear as a very narrow peak in the invariant mass distribution of the two photons (see Fig. 1 as an example for the CC sample). The diphoton mass resolution, as determined from simulation and checked using $Z \rightarrow e^+e^-$ decays in data, is better than 3 GeV/ c^2 for the Higgs boson mass regions and diphoton channels studied here and is limited by the energy resolution of the EM calorimeters [36]. The mass resolution is also sensitive to the selection of the correct primary vertex of the $p\bar{p}$ interac-

TABLE II. Expected and observed 95% C.L. upper limits on the production cross section times branching ratio relative to the SM prediction, the production cross section times branching ratio with theoretical cross section uncertainties removed, and the h_f branching ratio. The fermiophobic benchmark model prediction for $\mathcal{B}(h_f \rightarrow \gamma\gamma)$ is also shown for comparison.

	m_H (GeV/ c^2)	100	105	110	115	120	125	130	135	140	145	150
$\sigma \times \mathcal{B}(H \rightarrow \gamma\gamma)/\text{SM}$	Expected	16.4	14.8	14.2	13.8	13.3	13.6	14.4	15.8	17.7	20.8	27.5
	Observed	15.1	13.9	8.5	14.6	28.7	19.2	19.2	14.8	23.1	21.9	21.4
$\sigma \times \mathcal{B}(H \rightarrow \gamma\gamma)$ (fb)	Expected	57.3	50.8	47.9	43.2	39.0	36.0	32.8	30.6	28.5	26.7	26.1
	Observed	52.9	47.8	28.8	44.8	84.4	50.4	44.7	29.4	36.9	28.0	20.2
$\mathcal{B}(h_f \rightarrow \gamma\gamma)$ (%)	Expected	4.4	4.9	5.2	5.8	6.0	6.4	6.8	7.4	7.7	8.1	8.7
	Observed	4.8	5.4	2.8	4.2	7.3	5.5	6.6	6.6	5.7	7.8	8.1
	Fermiophobic Prediction	18.2	10.6	6.2	3.8	2.8	2.2	1.9	1.2	0.6	0.3	0.2

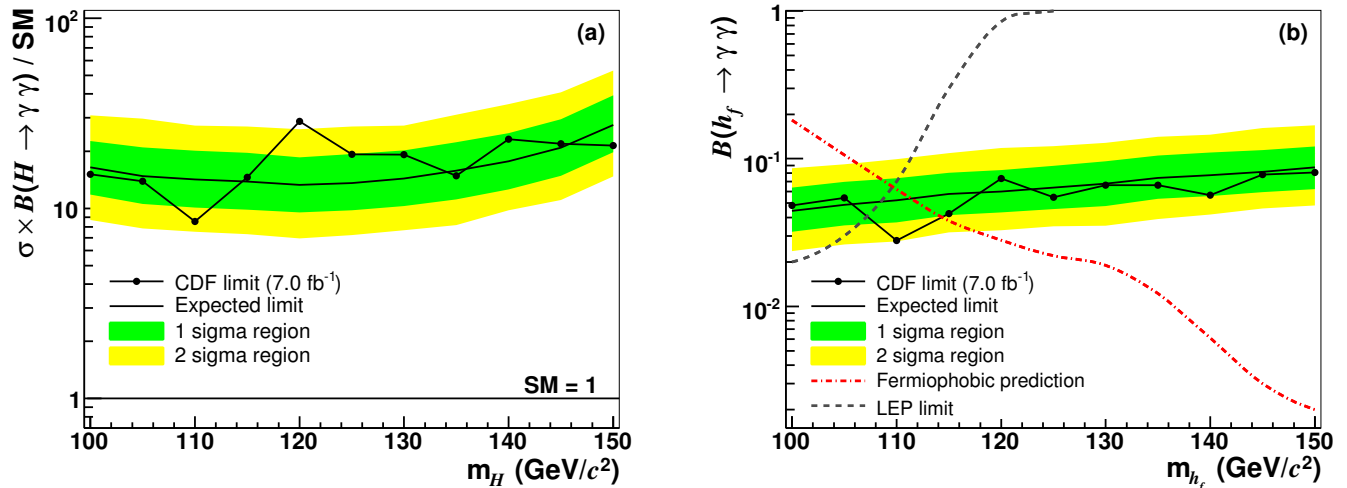


FIG. 2. (a) As a function of m_H , the 95% C.L. upper limit on cross section times branching ratio for the SM Higgs boson decay to two photons, relative to the SM prediction. (b) The 95% C.L. upper limit on the branching ratio for the fermiophobic Higgs boson decay to two photons, as a function of m_{h_f} . For reference, the 95% C.L. limits from LEP are also included. The shaded regions represent the 1σ and 2σ probability of fluctuations of the observed limit away from the expected limit based on the distribution of simulated experimental outcomes.

tion, determined by selecting the vertex with the highest sum of associated track momenta. The locations of the vertex and EM energy cluster are used to derive the photon's momentum. For GF (VH and VBF) signal samples, the primary vertex is misidentified in roughly 16% (4%) of nonconversion channel (CC and CP) events, which degrades the resolution of the reconstructed Higgs boson mass [37]. This effect is studied using Z decays in the data and found to be well-modeled in the simulation.

The total background prediction is estimated from a fit made to the data using a binned log-likelihood ($\log \ell$) method [38]. The fit is performed for each m_H hypothesis in 5 GeV/ c^2 steps from 100 to 150 GeV/ c^2 . At each step, a 12 GeV/ c^2 mass window centered on the point is excluded, where 12 GeV/ c^2 is chosen to include 95% of the signal. Fits for a m_H hypothesis of 120 GeV/ c^2 are shown in Fig. 1. The statistical uncertainties on the total background in the signal region, taken from the fit, are 8% or less for the channels associated with the SM Higgs

boson search and 12% or less for the channels associated with the fermiophobic Higgs boson search (except for the channels associated with the high- $p_T^{\gamma\gamma}$ bins with conversion photons, where it is 27%).

No obvious evidence of a narrow peak or any other anomalous structure is visible in the diphoton mass spectrum. We calculate a Bayesian C.L. limit for each Higgs boson mass hypothesis based on a combination of binned likelihoods for all channels using six bins in the 12 GeV/ c^2 signal region (2 GeV/ c^2 bin width) of each mass distribution. We use a flat prior in $\sigma \times \mathcal{B}(H \rightarrow \gamma\gamma)$ and integrate over the priors for the systematic uncertainties. A 95% C.L. limit is determined such that 95% of the posterior density for $\sigma \times \mathcal{B}(H \rightarrow \gamma\gamma)$ falls below the limit [39]. The expected 95% C.L. limits are calculated assuming no signal, based on expected backgrounds only, as the median of 2000 simulated experiments. The observed 95% C.L. on $\sigma \times \mathcal{B}(H \rightarrow \gamma\gamma)$ are calculated from the data. The limit results are displayed in Table II and graphically in Fig. 2. For a SM Higgs boson, the re-

sults are shown relative to the theory prediction, where theoretical cross section uncertainties of 14% on the GF process, 6% on the VH process, and 5% on the VBF process are included in the limit calculation [40, 41]. Limits are also provided on $\sigma \times \mathcal{B}(H \rightarrow \gamma\gamma)$ without including theoretical cross section uncertainties. The inclusion of systematic uncertainties in the SM (fermiophobic) limit calculation degrades the limit on $\sigma \times \mathcal{B}(H \rightarrow \gamma\gamma)$ by 15% (9%), where the effect of the uncertainty on the background estimate is dominant at 10% (6%).

For the SM limit at $m_H = 120 \text{ GeV}/c^2$, we observe a deviation of greater than 2.5σ from the expectation [42]. After accounting for the trials factor associated with performing the search at 11 mass points, the significance of this discrepancy decreases to less than 2σ . When the analysis is optimized for the fermiophobic benchmark model, no excess is observed. For the h_f model, SM cross sections and uncertainties are assumed (GF excluded) and used to convert limits on $\sigma \times \mathcal{B}(h_f \rightarrow \gamma\gamma)$ into limits on $\mathcal{B}(h_f \rightarrow \gamma\gamma)$. Table II gives the predicted $\mathcal{B}(h_f \rightarrow \gamma\gamma)$ for this model as calculated using HDECAY [2]. We obtain a lower limit on m_{h_f} of $114 \text{ GeV}/c^2$ by linear interpolation between the sampled values of m_{h_f} based on the intersection of the observed limit and the model prediction.

This Letter presents the results of a search for a narrow resonance in the diphoton mass spectrum using data taken by the CDF II detector at the Tevatron. We have improved upon the previous CDF analysis by implementing a neural network discriminant to improve central photon identification, recovering central photons that have converted to an e^+e^- pair, and more than doubling the amount of data analyzed. There is no significant evidence of a resonance in the data. Limits are placed on the production cross section times branching ratio for Higgs boson decay into a photon pair and compared to the predictions of the standard model and a benchmark fermiophobic model. The latter result excludes fermiophobic Higgs boson masses below $114 \text{ GeV}/c^2$ at the 95% C.L., which is the strongest limit to date on this model by a single experiment.

We thank the Fermilab staff and the technical staffs of the participating institutions for their vital contributions. This work was supported by the U.S. Department of Energy and National Science Foundation; the Italian Istituto Nazionale di Fisica Nucleare; the Ministry of Education, Culture, Sports, Science, and Technology of Japan; the Natural Sciences and Engineering Research Council of Canada; the National Science Council of the Republic of China; the Swiss National Science Foundation; the A.P. Sloan Foundation; the Bundesministerium für Bildung und Forschung, Germany; the Korean World Class University Program and the National Research Foundation of Korea; the Science and Technology Facilities Council and the Royal Society, UK; the Institut National de Physique Nucleaire et Physique des

Particules/CNRS of France; the Russian Foundation for Basic Research; the Ministerio de Ciencia e Innovación and Programa Consolider-Ingenio 2010, Spain; the Slovak R&D Agency; the Academy of Finland; and the Australian Research Council (ARC).

* Deceased

† With visitors from ^aIstituto Nazionale di Fisica Nucleare, Sezione di Cagliari, 09042 Monserrato (Cagliari), Italy, ^bUniversity of California Irvine, Irvine, CA 92697, USA, ^cUniversity of California Santa Barbara, Santa Barbara, CA 93106, USA, ^dUniversity of California Santa Cruz, Santa Cruz, CA 95064, USA, ^eCERN, CH-1211 Geneva, Switzerland, ^fCornell University, Ithaca, NY 14853, USA, ^gUniversity of Cyprus, Nicosia CY-1678, Cyprus, ^hOffice of Science, U.S. Department of Energy, Washington, DC 20585, USA, ⁱUniversity College Dublin, Dublin 4, Ireland, ^jUniversity of Fukui, Fukui City, Fukui Prefecture, Japan 910-0017, ^kUniversidad Iberoamericana, Mexico D.F., Mexico, ^lIowa State University, Ames, IA 50011, USA, ^mUniversity of Iowa, Iowa City, IA 52242, USA, ⁿKinki University, Higashi-Osaka City, Japan 577-8502, ^oKansas State University, Manhattan, KS 66506, USA, ^pUniversity of Manchester, Manchester M13 9PL, United Kingdom, ^qQueen Mary, University of London, London, E1 4NS, United Kingdom, ^rUniversity of Melbourne, Victoria 3010, Australia, ^sMuons, Inc., Batavia, IL 60510, USA, ^tNagasaki Institute of Applied Science, Nagasaki, Japan, ^uNational Research Nuclear University, Moscow, Russia, ^vUniversity of Notre Dame, Notre Dame, IN 46556, USA, ^wUniversidad de Oviedo, E-33007 Oviedo, Spain, ^xTexas Tech University, Lubbock, TX 79609, USA, ^yUniversidad Tecnica Federico Santa Maria, 110v Valparaiso, Chile, ^zYarmouk University, Irbid 211-63, Jordan, ^{hh}On leave from J. Stefan Institute, Ljubljana, Slovenia.

- [1] P. W. Higgs, *Phys. Rev. Lett.* **13**, 508 (1964); G. S. Guralnik, C. R. Hagen, and T. W. B. Kibble, *Phys. Rev. Lett.* **13**, 585 (1964); F. Englert and R. Brout, *Phys. Rev. Lett.* **13**, 321 (1964).
- [2] A. Djouadi, J. Kalinowski, and M. Spira, *Comput. Phys. Commun.* **108**, 56 (1998).
- [3] Tevatron New Phenomena and Higgs Working Group (CDF and D0 Collaborations), [arXiv:1107.5518](https://arxiv.org/abs/1107.5518).
- [4] LEP, Tevatron, and SLD Electroweak Working Groups, [arXiv:1012.2367](https://arxiv.org/abs/1012.2367).
- [5] A. Rosca (LEP Collaborations), *Nucl. Phys. B, Proc. Suppl.* **117**, 743 (2003); A. G. Akeroyd, *Phys. Lett. B* **368**, 89 (1996); A. Barroso, L. Brücher, and R. Santos, *Phys. Rev. D* **60**, 035005 (1999); S. Mrenna and J. Wells, *Phys. Rev. D* **63**, 015006 (2000); H. E. Haber, G. L. Kane, and T. Sterling, *Nucl. Phys. B* **161**, 493 (1979); J. F. Gunion, R. Vega, and J. Wudka, *Phys. Rev. D* **42**, 1673 (1990); V. Barger, N. G. Deshpande, J. L. Hewett, and T. G. Rizzo, [arXiv:hep-ph/9211234](https://arxiv.org/abs/hep-ph/9211234); J.-L. Basdevant, E. L. Berger, D. Dicus, C. Kao, and S. Willenbrock, *Phys. Lett. B* **313**, 402 (1993); A. Stange, W. Marciano, and S. Willenbrock, *Phys. Rev. D* **49**, 1354 (1994); M. A. Díaz and T. J. Weiler, [arXiv:hep-ph/9401259](https://arxiv.org/abs/hep-ph/9401259); L. Brücher and R. Santos, *Eur. Phys. J. C*

- 12, 87 (2000); G. Landsberg and K. T. Matchev, *Phys. Rev. D* **62**, 035004 (2000).
- [6] T. Affolder *et al.* (CDF Collaboration), *Phys. Rev. D* **64**, 092002 (2001).
- [7] B. Abbott *et al.* (D0 Collaboration), *Phys. Rev. Lett.* **82**, 2244 (1999).
- [8] V. M. Abazov *et al.* (D0 Collaboration), *Phys. Rev. Lett.* **101**, 051801 (2008).
- [9] V. M. Abazov *et al.* (D0 Collaboration), *Phys. Rev. Lett.* **107**, 151801 (2011).
- [10] T. Aaltonen *et al.* (CDF Collaboration), *Phys. Rev. Lett.* **103**, 061803 (2009).
- [11] C. Anastasiou, R. Boughezal, and F. Petriello, *J. High Energy Phys.* **04** (2009) 003; D. de Florian and M. Grazzini, *Phys. Lett. B* **674**, 291 (2009).
- [12] J. Baglio and A. Djouadi, *J. High Energy Phys.* **10** (2010) 064; O. Brein, A. Djouadi, and R. Harlander, *Phys. Lett. B* **579**, 149 (2004); M. L. Ciccolini, S. Dittmaier, and M. Krämer, *Phys. Rev. D* **68**, 073003 (2003).
- [13] P. Bolzoni, F. Maltoni, S.-O. Moch, and M. Zaro, *Phys. Rev. Lett.* **105**, 011801 (2010); M. Ciccolini, A. Denner, and S. Dittmaier, *Phys. Rev. Lett.* **99**, 161803 (2007); *Phys. Rev. D* **77**, 013002 (2008).
- [14] D. Acosta *et al.* (CDF Collaboration), *Phys. Rev. D* **71**, 032001 (2005).
- [15] A. Sill (CDF Collaboration), *Nucl. Instrum. Methods Phys. Res., Sect. A* **447**, 1 (2000).
- [16] T. Affolder *et al.*, *Nucl. Instrum. Methods Phys. Res., Sect. A* **526**, 249 (2004).
- [17] L. Balka *et al.*, *Nucl. Instrum. Methods Phys. Res., Sect. A* **267**, 272 (1988).
- [18] S. Bertolucci *et al.*, *Nucl. Instrum. Methods Phys. Res., Sect. A* **267**, 301 (1988).
- [19] M. Albrow *et al.*, *Nucl. Instrum. Methods Phys. Res., Sect. A* **480**, 524 (2002).
- [20] CDF uses a cylindrical coordinate system with $+z$ in the proton beam direction. θ and ϕ are the polar and azimuthal angles, respectively, and pseudorapidity is $\eta = -\ln \tan(\theta/2)$.
- [21] G. Apollinari, K. Goulianos, P. Melese, and M. Lindgren, *Nucl. Instrum. Methods Phys. Res., Sect. A* **412**, 515 (1998).
- [22] The transverse energy E_T and transverse momentum p_T are defined as $E \sin \theta$ and $|\vec{p}| \sin \theta$, respectively.
- [23] T. Aaltonen *et al.* (CDF Collaboration), *Phys. Rev. Lett.* **99**, 171801 (2007).
- [24] S. Wynne, Ph.D. thesis, University of Liverpool, [Fermilab Report No. FERMILAB-THESIS-2007-17, 2007].
- [25] T. Aaltonen *et al.* (CDF Collaboration), *Phys. Rev. D* **82**, 052005 (2010).
- [26] Typically, this occurs when a jet fragments into a π^0 or η particle that subsequently decays to multiple photons, which are then reconstructed as a single photon.
- [27] The variables also allow the NN method to be applied to electrons, which are used to calibrate ID efficiencies.
- [28] F. Abe *et al.* (CDF Collaboration), *Phys. Rev. D* **48**, 2998 (1993).
- [29] K. R. Bland, Ph.D. thesis, Baylor University, expected 2012; K. R. Bland (for the CDF and D0 Collaborations), [arXiv:1110.1747](https://arxiv.org/abs/1110.1747).
- [30] See Supplemental Material for additional information, including tables of values for other Higgs boson masses.
- [31] T. Sjöstrand, P. Edén, C. Friberg, L. Lönnblad, G. Miu, S. Mrenna, and E. Norrbin, *Comput. Phys. Commun.* **135**, 238 (2001).
- [32] D. Stump *et al.*, *J. High Energy Phys.* **10** (2003) 046.
- [33] D. Bourilkov, R. C. Group, and M. R. Whalley, [arXiv:hep-ph/0605240](https://arxiv.org/abs/hep-ph/0605240).
- [34] We constrain the rate of initial-state radiation using Drell-Yan events in data.
- [35] S. Mrenna and C.-P. Yuan, *Phys. Lett. B* **416**, 200 (1998).
- [36] The natural width of the Higgs boson is negligible.
- [37] In CC (CP) events, the resolution degrades by 15 (12)%.
- [38] The combined $p_T^{\gamma\gamma}$ data and low- $p_T^{\gamma\gamma}$ data are fit to a sum of two exponentials multiplied by a fractional-degree polynomial, where the degree of one term is a parameter of the fit and the two higher $p_T^{\gamma\gamma}$ regions are fit to a simpler third-degree polynomial times an exponential. Channels with a plug photon have a non-negligible contamination from Z boson decays and additionally include a Breit-Wigner function to model this background.
- [39] K. Nakamura *et al.* (Particle Data Group), *J. Phys. G* **37**, 075021 (2010).
- [40] M. Botje *et al.*, [arXiv:1101.0538](https://arxiv.org/abs/1101.0538).
- [41] S. Dittmaier *et al.* (LHC Higgs Cross Section Working Group), [arXiv:1101.0593](https://arxiv.org/abs/1101.0593).
- [42] The LEP Working Group for Higgs Boson Searches (LEP Collaborations), *Phys. Lett. B* **565**, 61 (2003).

Supplemental Material
for
Search for a Higgs Boson in the Diphoton Final State
in $p\bar{p}$ Collisions at $\sqrt{s} = 1.96$ TeV

The CDF Collaboration

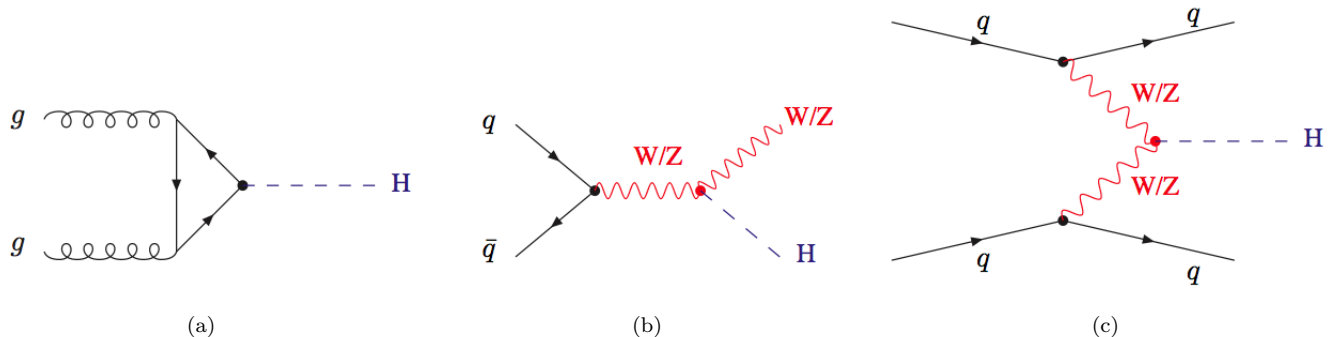


FIG. 1. The dominant production mechanisms at the Tevatron for the standard model (SM) Higgs boson: (a) gluon fusion (GF), (b) associated production (VH) where a Higgs boson is produced in association with a W or Z vector boson, and (c) vector boson fusion (VBF). For the fermiophobic Higgs boson h_f considered in this analysis, SM couplings are assumed; however, the gluon fusion process is suppressed and is therefore not included.

TABLE I. Production cross sections for the SM Higgs boson are given for the GF, VH ($V = W$ or Z), and VBF production mechanisms shown in Fig. 1. For h_f , the GF mechanism is excluded. The branching ratios for the decay to a photon pair are also shown for both the SM and fermiophobic Higgs boson.

M_H (GeV/ c^2)	σ_{GF} (fb)	σ_{WH} (fb)	σ_{ZH} (fb)	σ_{VBF} (fb)	$B(H \rightarrow \gamma\gamma)$ (%)	$B(h_f \rightarrow \gamma\gamma)$ (%)
100	1821.8	291.9	169.8	100.1	0.15	18.2
105	1584.7	248.4	145.9	92.3	0.17	10.6
110	1385.0	212.0	125.7	85.1	0.19	6.2
115	1215.9	174.5	103.9	78.6	0.20	3.8
120	1072.3	150.1	90.2	72.7	0.22	2.8
125	949.3	129.5	78.5	67.1	0.22	2.2
130	842.9	112.0	68.5	62.1	0.22	1.9
135	750.8	97.2	60.0	57.5	0.21	1.2
140	670.6	84.6	52.7	53.2	0.19	0.6
145	600.6	73.7	46.3	49.4	0.17	0.3
150	539.1	64.4	40.8	45.8	0.14	0.2

STANDARD MODEL HIGGS BOSON SEARCH

TABLE II. The SM Higgs boson search is divided into four independent categories (CC, CP, C'C, and C'P) as defined in the primary text of this Letter. For each SM Higgs boson mass hypotheses tested in this analysis, the efficiency multiplied by signal acceptance (ϵA) is shown as a percentage of the total number of $H \rightarrow \gamma\gamma$ decays for each production mechanism (GF, VH, and VBF). These values, along with the cross sections and branching ratios provided in Table I, are used to obtain the predicted number of SM Higgs boson signal events. The CC and C'C (CP and C'P) channels use data corresponding to an integrated luminosity of 7.0 fb^{-1} (6.7 fb^{-1}). The number of background and data events are also given for each mass. The final column in each subtable is the number of signal events divided by the square root of the number of background events (S/\sqrt{B}). The event yields for each mass point are obtained from a $12 \text{ GeV}/c^2$ signal region centered on the Higgs boson mass hypothesis, allowing a $2 \text{ GeV}/c^2$ overlap between signal regions.

(a)								(b)									
CC Channel				CDF Run II, 7.0 fb^{-1}				CP Channel				CDF Run II, 6.7 fb^{-1}					
m_H	ϵA (%)			H_{SM}	Signal	Background	Data	S/\sqrt{B}	m_H	ϵA (%)			H_{SM}	Signal	Background	Data	S/\sqrt{B}
(GeV/c^2)	GF	VH	VBF						(GeV/c^2)	GF	VH	VBF					
100	9.8	10.1	11.0	2.5	621	615	0.10		100	11.5	10.3	10.3	2.7	4296	4244	0.04	
105	9.9	10.0	11.0	2.5	526	502	0.11		105	11.7	10.4	10.6	2.7	3580	3613	0.04	
110	9.9	10.2	11.0	2.4	414	400	0.12		110	11.9	10.6	10.8	2.7	2919	2851	0.05	
115	9.9	10.2	11.0	2.2	346	361	0.12		115	11.9	10.8	10.9	2.5	2547	2472	0.05	
120	10.0	10.2	11.0	2.2	271	308	0.13		120	12.0	10.9	11.1	2.4	2071	2075	0.05	
125	10.0	10.2	10.9	1.9	237	279	0.12		125	12.0	10.8	11.1	2.1	1819	1866	0.05	
130	10.1	10.2	11.1	1.7	197	207	0.12		130	11.9	10.8	11.1	1.9	1511	1506	0.05	
135	10.0	10.1	10.9	1.4	177	181	0.11		135	11.9	10.9	11.1	1.6	1332	1359	0.04	
140	10.2	10.3	11.1	1.2	144	150	0.10		140	11.7	10.8	11.0	1.3	1118	1093	0.04	
145	10.2	10.1	10.9	0.9	128	129	0.08		145	11.8	10.8	11.0	1.0	992	964	0.03	
150	10.2	10.2	11.0	0.7	112	99	0.07		150	11.6	10.7	10.9	0.7	825	851	0.03	

(c)								(d)									
C'C Channel				CDF Run II, 7.0 fb^{-1}				C'P Channel				CDF Run II, 6.7 fb^{-1}					
m_H	ϵA (%)			H_{SM}	Signal	Background	Data	S/\sqrt{B}	m_H	ϵA (%)			H_{SM}	Signal	Background	Data	S/\sqrt{B}
(GeV/c^2)	GF	VH	VBF						(GeV/c^2)	GF	VH	VBF					
100	2.3	2.2	2.5	0.6	159	158	0.05		100	1.3	1.0	1.1	0.3	671	652	0.01	
105	2.3	2.2	2.5	0.6	126	141	0.05		105	1.3	1.2	1.2	0.3	466	443	0.01	
110	2.3	2.3	2.6	0.6	107	92	0.05		110	1.3	1.1	1.2	0.3	328	356	0.02	
115	2.3	2.2	2.5	0.5	87.8	80	0.05		115	1.3	1.1	1.2	0.3	280	318	0.02	
120	2.4	2.3	2.6	0.5	66.5	67	0.06		120	1.4	1.2	1.2	0.3	225	268	0.02	
125	2.4	2.2	2.5	0.4	58.8	55	0.06		125	1.4	1.2	1.2	0.2	204	235	0.02	
130	2.4	2.3	2.6	0.4	47.4	44	0.06		130	1.4	1.2	1.3	0.2	175	181	0.02	
135	2.4	2.2	2.5	0.3	40.7	39	0.05		135	1.4	1.2	1.3	0.2	160	140	0.01	
140	2.4	2.3	2.5	0.3	31.8	40	0.05		140	1.4	1.2	1.3	0.1	138	106	0.01	
145	2.3	2.2	2.4	0.2	29.1	38	0.04		145	1.4	1.2	1.3	0.1	120	104	0.01	
150	2.4	2.3	2.6	0.2	27.1	23	0.03		150	1.4	1.2	1.3	0.1	101	99	0.01	

FERMIOPHOBIC HIGGS BOSON SEARCH

(A) $p_T^{\gamma\gamma} > 75$ GeV/c Region

TABLE III. The fermiophobic Higgs boson search is divided into four independent categories (CC, CP, C'C, and C'P) as in the SM Higgs boson search, and it is additionally divided into three regions of $p_T^{\gamma\gamma}$. The $p_T^{\gamma\gamma} > 75$ GeV/c region is shown here, which provides the greatest sensitivity for a fermiophobic Higgs boson observation. For each h_f mass hypotheses tested in this analysis, the efficiency multiplied by signal acceptance (ϵA) is shown as a percentage of the total number of $H \rightarrow \gamma\gamma$ decays for each production mechanism (VH and VBF). These values, along with the cross sections and branching ratios provided in Table I, are used to obtain the predicted number of SM Higgs boson signal events. The CC and C'C (CP and C'P) channels use data corresponding to an integrated luminosity of 7.0 fb^{-1} (6.7 fb^{-1}). The number of background and data events are also given for each mass. The final column in each subtable is the number of signal events divided by the square root of the number of background events (S/\sqrt{B}). The event yields for each mass point are obtained from a $12 \text{ GeV}/c^2$ signal region centered on the Higgs boson mass hypothesis, allowing a $2 \text{ GeV}/c^2$ overlap between signal regions.

(a)							(b)								
CC Channel, $p_T^{\gamma\gamma} > 75$ GeV				CDF Run II, 7.0 fb^{-1}			CP Channel, $p_T^{\gamma\gamma} > 75$ GeV				CDF Run II, 6.7 fb^{-1}				
m_{h_f} (GeV/ c^2)	ϵA (%)		h_f	Signal	Background	Data	S/\sqrt{B}	m_{h_f} (GeV/ c^2)	ϵA (%)		h_f	Signal	Background	Data	S/\sqrt{B}
	VH	VBF							VH	VBF					
100	4.14	4.03	29.5	29.8	32	5.4		100	3.18	2.97	21.5	69.3	76	2.6	
105	4.32	4.10	15.4	29.7	27	2.8		105	3.36	3.09	11.4	67.6	73	1.4	
110	4.58	4.14	8.2	25.3	23	1.6		110	3.60	3.32	6.2	66.0	63	0.8	
115	4.71	4.18	4.4	22.6	21	0.9		115	3.96	3.37	3.5	64.0	58	0.4	
120	4.82	4.18	2.9	19.1	21	0.7		120	4.20	3.58	2.4	60.6	50	0.3	
125	4.99	4.18	2.0	16.6	23	0.5		125	4.40	3.62	1.7	59.0	35	0.2	
130	5.15	4.25	1.6	15.3	16	0.4		130	4.55	3.72	1.3	52.4	46	0.2	
135	5.22	4.24	0.9	14.6	10	0.2		135	4.78	3.79	0.8	47.9	51	0.1	
140	5.49	4.31	0.4	12.9	7	0.1		140	4.98	3.80	0.4	43.3	51	0.05	
145	5.47	4.27	0.2	11.5	8	0.05		145	5.15	3.89	0.2	41.0	42	0.03	
150	5.65	4.37	0.1	9.7	7	0.04		150	5.21	3.89	0.1	38.1	36	0.02	

(c)							(d)								
C'C Channel, $p_T^{\gamma\gamma} > 75$ GeV				CDF Run II, 7.0 fb^{-1}			C'P Channel, $p_T^{\gamma\gamma} > 75$ GeV				CDF Run II, 6.7 fb^{-1}				
m_{h_f} (GeV/ c^2)	ϵA (%)		h_f	Signal	Background	Data	S/\sqrt{B}	m_{h_f} (GeV/ c^2)	ϵA (%)		h_f	Signal	Background	Data	S/\sqrt{B}
	VH	VBF							VH	VBF					
100	0.83	0.83	5.9	5.2	8	2.6		100	0.27	0.28	1.9	8.0	6	0.7	
105	0.84	0.84	3.0	4.6	7	1.4		105	0.31	0.30	1.1	7.6	5	0.4	
110	0.93	0.88	1.7	5.5	3	0.7		110	0.35	0.31	0.6	6.0	7	0.2	
115	0.93	0.88	0.9	5.2	1	0.4		115	0.35	0.31	0.3	5.9	5	0.1	
120	1.02	0.87	0.6	4.4	2	0.3		120	0.40	0.33	0.2	6.0	4	0.09	
125	1.02	0.87	0.4	4.0	2	0.2		125	0.41	0.33	0.2	5.6	4	0.07	
130	1.06	0.89	0.3	2.8	4	0.2		130	0.42	0.36	0.1	5.6	2	0.05	
135	1.05	0.88	0.2	2.2	5	0.1		135	0.46	0.38	0.08	5.0	2	0.03	
140	1.12	0.90	0.1	2.2	3	0.06		140	0.47	0.39	0.03	4.3	4	0.02	
145	1.14	0.86	0.04	2.0	2	0.03		145	0.48	0.38	0.02	3.5	5	0.01	
150	1.14	0.95	0.02	2.0	1	0.02		150	0.51	0.40	0.01	2.7	7	0.01	

(B) $35 < p_T^{\gamma\gamma} < 75$ GeV/ c Region

TABLE IV. The fermiophobic Higgs boson search is divided into four independent categories (CC, CP, C'C, and C'P) as in the SM Higgs boson search, and it is additionally divided into three regions of $p_T^{\gamma\gamma}$. The $35 < p_T^{\gamma\gamma} < 75$ GeV/ c region is shown here. For each h_f mass hypotheses tested in this analysis, the efficiency multiplied by signal acceptance (ϵA) is shown as a percentage of the total number of $H \rightarrow \gamma\gamma$ decays for each production mechanism (VH and VBF). These values, along with the cross sections and branching ratios provided in Table I, are used to obtain the predicted number of SM Higgs boson signal events. The CC and C'C (CP and C'P) channels use data corresponding to an integrated luminosity of 7.0 fb^{-1} (6.7 fb^{-1}). The number of background and data events are also given for each mass. The final column in each subtable is the number of signal events divided by the square root of the number of background events (S/\sqrt{B}). The event yields for each mass point are obtained from a $12 \text{ GeV}/c^2$ signal region centered on the Higgs boson mass hypothesis, allowing a $2 \text{ GeV}/c^2$ overlap between signal regions.

(a)							(b)						
CC Channel, $35 < p_T^{\gamma\gamma} < 75$ GeV/ c CDF Run II, 7.0 fb^{-1}							CP Channel, $35 < p_T^{\gamma\gamma} < 75$ GeV/ c CDF Run II, 6.7 fb^{-1}						
m_{h_f} (GeV/ c^2)	ϵA (%)		h_f		Data	S/\sqrt{B}	m_{h_f} (GeV/ c^2)	ϵA (%)		h_f		Data	S/\sqrt{B}
	VH	VBF	Signal	Background			VH	VBF	Signal	Background	Data		
100	4.00	4.61	29.4	97.0	101	3.0	100	4.80	4.91	33.0	546	554	1.4
105	3.87	4.55	14.4	83.2	78	1.6	105	4.88	5.01	16.9	501	485	0.8
110	3.87	4.62	7.4	64.7	69	0.9	110	4.84	4.97	8.5	439	413	0.4
115	3.83	4.63	3.8	57.7	51	0.5	115	4.77	5.03	4.4	398	362	0.2
120	3.78	4.60	2.4	43.9	47	0.4	120	4.75	5.01	2.8	344	316	0.2
125	3.66	4.57	1.6	37.4	41	0.3	125	4.63	5.08	1.9	312	275	0.1
130	3.67	4.63	1.3	30.5	31	0.2	130	4.55	4.97	1.4	263	260	0.09
135	3.56	4.58	0.7	27.6	24	0.1	135	4.46	4.99	0.8	232	253	0.05
140	3.52	4.60	0.3	22.7	18	0.06	140	4.33	4.96	0.3	203	193	0.02
145	3.43	4.51	0.1	18.3	18	0.03	145	4.30	4.84	0.2	182	180	0.01
150	3.41	4.57	0.08	15.1	18	0.02	150	4.17	4.74	0.1	154	158	0.01

(c)							(d)						
C'C Channel, $35 < p_T^{\gamma\gamma} < 75$ GeV/ c CDF Run II, 7.0 fb^{-1}							C'P Channel, $35 < p_T^{\gamma\gamma} < 75$ GeV/ c CDF Run II, 6.7 fb^{-1}						
m_{h_f} (GeV/ c^2)	ϵA (%)		h_f		Data	S/\sqrt{B}	m_{h_f} (GeV/ c^2)	ϵA (%)		h_f		Data	S/\sqrt{B}
	VH	VBF	Signal	Background			VH	VBF	Signal	Background	Data		
100	0.87	1.00	6.4	21.3	21	1.4	100	0.46	0.47	3.16	77.7	73	0.36
105	0.86	1.03	3.2	18.9	19	0.7	105	0.50	0.53	1.75	65.0	57	0.22
110	0.86	1.05	1.6	16.2	14	0.4	110	0.48	0.50	0.85	51.7	50	0.12
115	0.85	1.05	0.8	13.9	13	0.2	115	0.48	0.53	0.45	42.7	50	0.07
120	0.87	1.04	0.6	10.2	16	0.2	120	0.48	0.52	0.29	32.3	50	0.05
125	0.82	1.03	0.4	9.4	12	0.1	125	0.50	0.51	0.20	32.9	42	0.04
130	0.83	1.09	0.3	8.8	7	0.1	130	0.49	0.55	0.16	31.4	25	0.03
135	0.79	1.02	0.2	7.9	4	0.06	135	0.46	0.52	0.08	28.5	22	0.02
140	0.80	1.04	0.07	6.4	5	0.03	140	0.45	0.52	0.04	25.6	13	0.01
145	0.74	1.04	0.03	5.5	5	0.01	145	0.45	0.54	0.02	20.6	16	0.004
150	0.76	1.04	0.02	4.0	6	0.01	150	0.46	0.52	0.01	16.1	20	0.002

(C) $p_T^{\gamma\gamma} < 35 \text{ GeV}/c$ Region

TABLE V. The fermiophobic Higgs boson search is divided into four independent categories (CC, CP, C'C, and C'P) as in the SM Higgs boson search, and it is additionally divided into three regions of $p_T^{\gamma\gamma}$. The $p_T^{\gamma\gamma} < 35 \text{ GeV}/c$ region is shown here. For each h_f mass hypotheses tested in this analysis, the efficiency multiplied by signal acceptance (ϵA) is shown as a percentage of the total number of $H \rightarrow \gamma\gamma$ decays for each production mechanism (VH and VBF). These values, along with the cross sections and branching ratios provided in Table I, are used to obtain the predicted number of SM Higgs boson signal events. The CC and C'C (CP and C'P) channels use data corresponding to an integrated luminosity of 7.0 fb^{-1} (6.7 fb^{-1}). The number of background and data events are also given for each mass. The final column in each subtable is the number of signal events divided by the square root of the number of background events (S/\sqrt{B}). The event yields for each mass point are obtained from a $12 \text{ GeV}/c^2$ signal region centered on the Higgs boson mass hypothesis, allowing a $2 \text{ GeV}/c^2$ overlap between signal regions.

(a)							(b)								
CC Channel, $p_T^{\gamma\gamma} < 35 \text{ GeV}/c$				CDF Run II, 7.0 fb^{-1}			CP Channel, $p_T^{\gamma\gamma} < 35 \text{ GeV}/c$				CDF Run II, 6.7 fb^{-1}				
m_{h_f} (GeV/c^2)	ϵA (%)		h_f	Signal	Background	Data	S/\sqrt{B}	m_{h_f} (GeV/c^2)	ϵA (%)		h_f	Signal	Background	Data	S/\sqrt{B}
	VH	VBF							VH	VBF					
100	2.30	2.66	16.9	490	482	0.76		100	2.92	3.08	20.2	3646	3614	0.33	
105	2.15	2.67	8.1	413	397	0.40		105	2.78	3.12	9.8	3014	3055	0.18	
110	2.09	2.64	4.0	328	308	0.22		110	2.73	3.07	4.9	2423	2375	0.10	
115	2.01	2.62	2.0	269	289	0.12		115	2.62	3.07	2.5	2100	2052	0.05	
120	1.92	2.60	1.3	214	240	0.09		120	2.48	3.02	1.5	1683	1709	0.04	
125	1.84	2.51	0.8	189	215	0.06		125	2.38	2.98	1.0	1463	1556	0.03	
130	1.77	2.55	0.6	156	160	0.05		130	2.28	2.94	0.8	1215	1200	0.02	
135	1.73	2.53	0.4	138	147	0.03		135	2.23	2.88	0.4	1071	1055	0.01	
140	1.64	2.54	0.2	110	125	0.01		140	2.06	2.82	0.2	886	849	0.006	
145	1.58	2.50	0.07	100	103	0.007		145	2.00	2.80	0.08	782	742	0.003	
150	1.52	2.50	0.04	88	74	0.004		150	1.92	2.76	0.04	643	657	0.002	

(c)							(d)								
C'C Channel, $p_T^{\gamma\gamma} < 35 \text{ GeV}/c$				CDF Run II, 7.0 fb^{-1}			C'P Channel, $p_T^{\gamma\gamma} < 35 \text{ GeV}/c$				CDF Run II, 6.7 fb^{-1}				
m_{h_f} (GeV/c^2)	ϵA (%)		h_f	Signal	Background	Data	S/\sqrt{B}	m_{h_f} (GeV/c^2)	ϵA (%)		h_f	Signal	Background	Data	S/\sqrt{B}
	VH	VBF							VH	VBF					
100	0.51	0.62	3.8	130	129	0.33		100	0.29	0.34	2.0	557	573	0.09	
105	0.51	0.61	1.9	99.6	115	0.19		105	0.31	0.35	1.1	395	381	0.06	
110	0.48	0.61	0.9	82.5	75	0.10		110	0.28	0.34	0.5	274	299	0.03	
115	0.43	0.57	0.4	66.6	66	0.05		115	0.28	0.33	0.3	234	263	0.02	
120	0.43	0.61	0.3	52.4	49	0.04		120	0.27	0.33	0.2	188	213	0.01	
125	0.42	0.57	0.2	45.8	41	0.03		125	0.27	0.33	0.1	167	188	0.009	
130	0.42	0.62	0.2	36.9	33	0.03		130	0.26	0.33	0.09	139	153	0.007	
135	0.38	0.59	0.08	32.2	30	0.01		135	0.24	0.32	0.05	127	116	0.004	
140	0.39	0.58	0.04	24.6	32	0.007		140	0.23	0.33	0.02	109	89	0.002	
145	0.37	0.57	0.02	23.0	31	0.003		145	0.23	0.33	0.009	95	83	0.001	
150	0.36	0.58	0.01	22.4	16	0.002		150	0.22	0.31	0.005	80	72	0.001	